Tectonophysics 814 (2021) 228973

Contents lists available at ScienceDirect

Tectonophysics

journal homepage: www.elsevier.com/locate/tecto

Crustal P-wave velocity structure and earthquake distribution in the Jiaodong Peninsula, China

Junhao Qu [a,b,*], Stephen S. Gao [b], Changzai Wang [c], Kelly H. Liu [b], Shaohui Zhou [a], Yuyong Yang [a], Yangang Sui [d], Zhengshuai Zhang [a]

[a] Shandong Earthquake Agency, Jinan 250102,China
[b] Geology and Geophysics Program, Missouri University of Science and Technology, Rolla MO65401, USA
[c] Institute of Geophysics, China Earthquake Administration, Beijing 100029, China
[d] Shandong Bureau of Coal Geology, Jinan, 250102, China

ARTICLE INFO

Keywords:
Jiaodong Peninsula
Double-difference tomography
Earthquake relocation
Seismic velocities
Fault zone structure

ABSTRACT

The Jiaodong Peninsula of eastern China is densely populated and prone to frequent moderate-strong earthquakes that are mostly distributed along a group of northeastern oriented Mesozoic-Cenozoic faults. An improved understanding of the seismic velocity structure in the area is of great significance for the roles that the faults played in the formation and evolution of the various tectonic features and for the assessment of future earthquake risks. By utilizing earthquake records of the Shandong Provincial Seismic Network for the period from January 2013 to January 2020, this study simultaneously re-locates earthquakes and determines the three-dimensional P-wave velocity structure beneath the Jiaodong Peninsula using regional P-wave travel times by applying the double-difference tomography method. After the relocation, the travel time residuals are reduced by an order of magnitude, and the epicenters are more concentrated and demonstrate a closer spatial relationship with known active faults. The resulting P-wave velocity structure at different horizon depths indicates lateral heterogeneities in the study area. Clear differences in the characteristics of velocity anomalies are observed between the Jiaobei Uplift, Jiaolai Basin and Sulu ultra-high pressure metamorphic belt. The anomalies are mostly NE oriented, which is consistent with the strike of the regional faults and may suggest structural control of the faults to the geological configurations. Earthquakes generally occurred along the edges of high or low velocity regions, and areas accommodating the intersections of the Penglai-Weihai, Penglai-Qixia and Mouping-Jimo fault zones have the greatest potential for future damaging earthquakes in the area.

1. Introduction

Situated along the eastern margin of the North China Craton, the Jiaodong Peninsula (JDP; Fig. 1) has experienced a complicated set of tectonic events since the Precambrian, among which the most significant ones include the collision between the North China and South China plates during the Indo-Chinese epoch (250–200 Ma) and the Yanshanian tectonic-magmatic activity (170–110 Ma). From the Paleozoic to the early Mesozoic, the dominant structural trends of the region changed from *E*-W to NNE-SSW, and the main tectonic regime varied from compressional to extensional (Meng, 2003; Fan et al., 2005; Xia et al., 2016).

A number of geophysical studies aimed at understanding the geological structure and seismicity of the JDP have been conducted (Ma, 1989; Wang et al., 2004; Wang et al., 2013a; Zhao et al., 2012; Pan et al., 2015; Zhang et al., 2018), which indicate that the JDP has a complex regional geological structure, with the coexistence of low-velocity and high-velocity blocks in the crust and upper mantle resulting from the intensive tectonic and magmatic activities. Pan et al. (2015) deployed a NW-SE oriented onshore-offshore seismic sounding profile in the eastern part of the peninsula and identified a close spatial correspondence between the deep and shallow structures. Su et al. (2016) conducted a study of the three-dimensional (3D) crustal P-wave velocity structure using 1369 earthquake records for the period 1975 to January 2014 in the Shandong region. The study shows that the blocks on both sides of the Tanlu Fault zone have different velocity structures, suggesting that the Tanlu Fault zone may be a boundary separating crust of different characteristics. The results indicate that the crust beneath the oceanic

* Corresponding author at: Shandong Earthquake Agency, Jinan 250102,China.
E-mail address: gisqjh@126.com (J. Qu).

https://doi.org/10.1016/j.tecto.2021.228973
Received 15 November 2020; Received in revised form 4 June 2021; Accepted 16 June 2021
Available online 18 June 2021

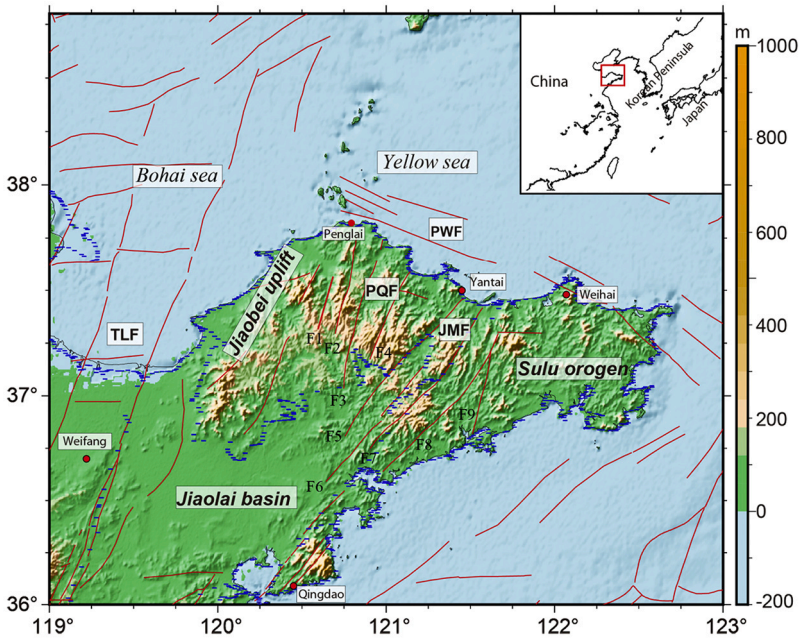

Fig. 1. Map of the JDP and adjacent areas showing major tectonic provinces and faults (Song, 2008). PWF: Penglai-Weihai faults, PQF: Penglai-Qixia faults, TLF: Tanlu fautls, JMF: Jimo-Muping faults. F1 is Beigou-Linglong fault, F2 is Fengyidian fault, F3 is Qixia fault, F4 is Bajiao-Shewopo fault, F5 is Taocun fault, F6 is Guocheng fault, F7 is Zhuwu fault, F8 is Haiyang fault, and F9 is Rushan fault.

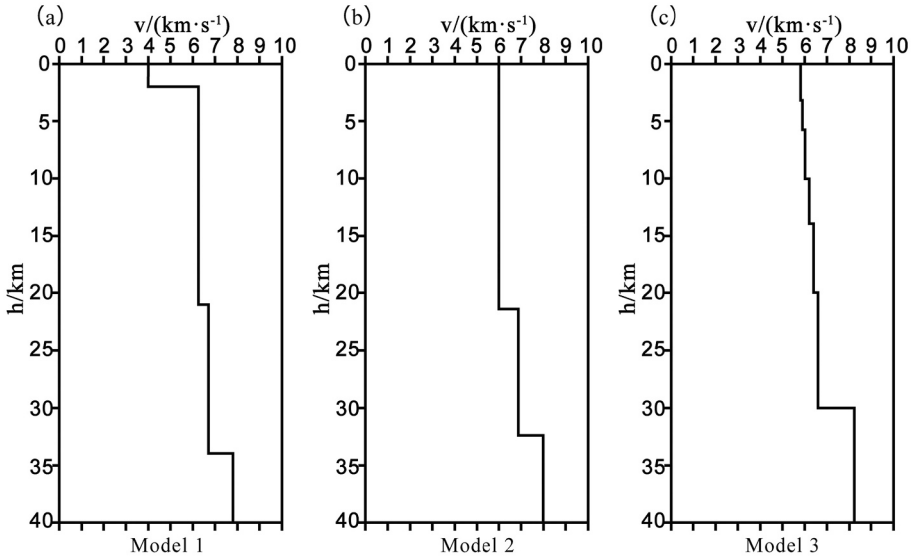

Fig. 2. 1D P-wave velocity models. (a) Study result of crustal velocity structure in Shandong area (Wang et al., 2007; Su et al., 2016; Xu et al., 2016; Wang et al., 2017); (b) Velocity model adopted by the Shandong seismic network; (3) Final velocity model used in this study (Wang et al., 2013a; Pan et al., 2015; Li et al., 2015).

Table 1
Reference crustal velocity model.

Depth(km)	Vp(km/s)	Vp/Vs
−10	0.30	1.76
3	5.80	
6	5.88	
10	5.99	
14	6.18	
20	6.38	
30	6.60	
> 30	8.10	

area north of the JDP, in the area of the Changdao swarm, is characterized by low P-wave velocities relative to the surrounding areas. These studies provided crucial references for understanding the geological structure and seismogenic background of the JDP.

Available historic records show that the JDP has experienced numerous moderate-strong earthquakes, including seven and five earthquakes with surface-wave magnitudes (Ms) exceeding 6.0 and 7.0, respectively (Pan et al., 2015). Recent improvements in seismic monitoring capability have recognized an apparent increase in the frequency of small and moderate earthquakes in the past decade, particularly the occurrence of earthquake swarms recorded in Changdao (2015; 2017–2018) and Rushan (2013–2020). The present study uses recordings of earthquakes from the Shandong Seismic Network for the period from January 2013 to January 2020 to relocate earthquakes and

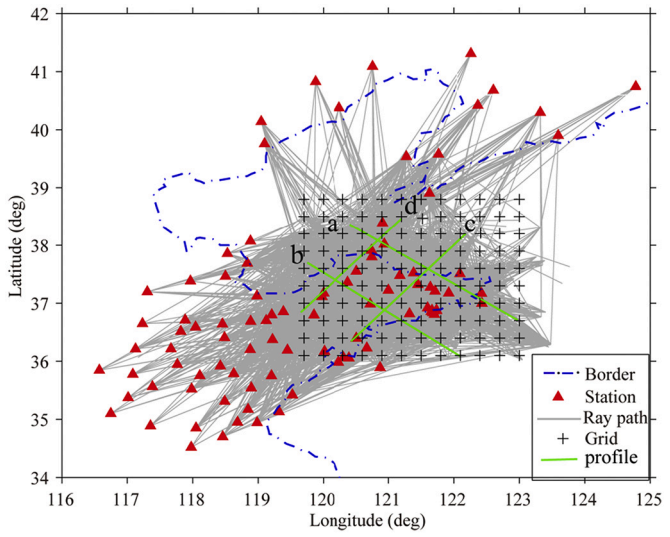

Fig. 3. Distributions of ray paths (gray lines) and stations (red triangles) in the study area. The green lines indicate the cross-sections shown in Fig. 10. (For interpretation of the references to colour in this figure legend, the reader is referred to the web version of this article.)

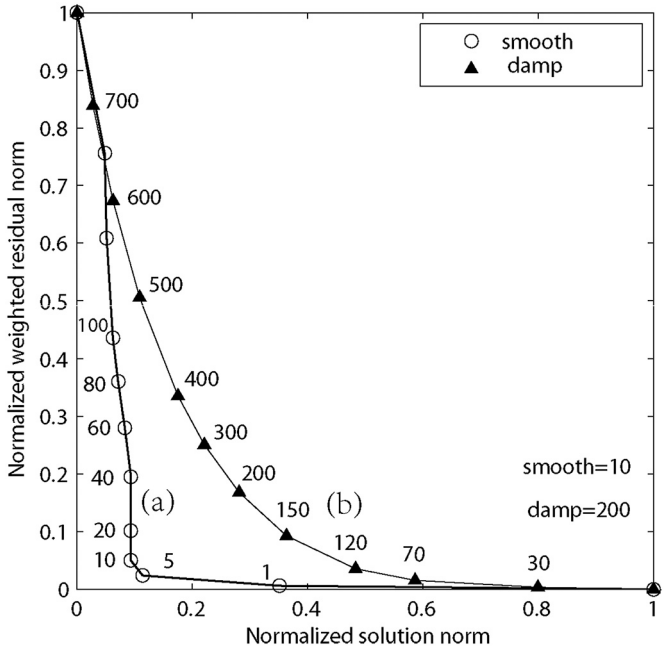

Fig. 4. Trade-off curves of damping and smoothing weight parameters for the smoothing (a) and damping (b) factors.

image the 3-D P-wave velocity structure in the JDP using the double-difference tomography method (Zhang and Thurber, 2003). The resulting earthquake locations and velocity structure, with improved accuracy and resolution relative to previous results, may provide valuable observational evidence for understanding the geological evolution and seismic activity of the region and for assessing and mitigating the risk of strong earthquakes in the future.

2. Overview of geological structure of the JDP

The JDP has a complex basement structure created by a series of tectonic events that led to tight folds and fault systems, accompanied by strong metamorphism and igneous activities. The JDP is composed of three major structural units (Fig. 1): the Jiaobei Uplift, the Jiaolai Basin and the Sulu ultra-high pressure (UHP) Metamorphic Belt (Guo et al., 2005; Qiu et al., 2008; Li et al., 2010; Xia et al., 2016). The Jiaobei Uplift mainly contains Precambrian metamorphic rocks and Mesozoic granites, along with small-scale Mesozoic and Cenozoic continental clastic rocks (Song and Wang, 2000; Guo et al., 2005; Xia et al., 2016). The Jiaolai Basin is a Late Mesozoic extensional basin, mainly composed of Cretaceous continental volcanic-sedimentary strata (Zhang et al., 2003). The Sulu UHP zone has Yangtze Craton properties and is well known for its high-pressure and ultra-high pressure metamorphic rocks (Song and Wang, 2000; Song et al., 2012; Tang et al., 2007; Guo et al., 2005; Li et al., 2006a).

Brittle faults, which are mostly oriented NNE-NE or NWW, are well developed in the JDP and adjacent areas (Fig. 1; Du, 2001, Du et al., 2001; Lin et al., 2003; Zhang et al., 2007; Huang et al., 2007; Ge et al., 2015). The NNE-NE trending fault system is the dominant fault structure in the JDP, and includes the Penglai-Qixia Fault Zone in the northwest and the Mouping-Jimo Fault Structural Zone slanting through the central part of the peninsula. The NNE-trending Penglai-Qixia Fault Zone extends to the south, and conceals under the Jiaolai Basin. It enters the North Yellow Sea to the north and intersects with the NWW-trending faults, some of which control the boundary of the Quaternary basins. The NE-NNE trending Jimo-Mouping Fault Zone intersects with the NWW-trending fault in the North Yellow Sea, and controls the formation and evolution of the Jiaolai Basin (Tang et al., 2003; Huang et al., 2007). Most of the faults have remained active since the Quaternary (Du et al., 2001; Ge et al., 2015). The NWW-trending faults, collectively called the Penglai-Weihai Fault, mainly distribute along the northern edge of the JDP and the oceanic area to the north, with strikes of 310°–320°. The faults form part of the southeastern section of the Zhangjiakou-Bohai Fault Structural Belt (Wang et al., 2006; Huang et al., 2007).

3. Methods

The double-difference tomography method employed in this study was developed by Zhang and Thurber (2003, 2006) based on the double-difference location method (Waldhauser and Ellsworth, 2000). This method combines absolute and relative arrival data to simultaneously relocate earthquakes and inverts for the velocity structure. The grid node method can be used to obtain the velocity of any point in space through the use of the difference in the velocities of adjacent nodes, and the pseudo-bending ray-tracing algorithm (Um and Thurber, 1987) is employed to determine the ray-path with the shortest travel time in a given event-station pair, following which the theoretical travel time and partial derivative of travel time to the hypocenter and slowness are calculated using the damped least squares algorithm (Paige and Saunders, 1982; VanDecar and Crosson, 1990). Different smoothing weights are used to constrain the model, and multiple iterations are conducted until a stable solution is obtained.

In contrast to the double-difference location method (Waldhauser and Ellsworth, 2000), the double-difference tomography method employed in the current study considers the spatial change in the velocity structure of the medium and does not require the assumption that the double-difference location has a constant velocity in the path between the station and the event pair. Moreover, the addition of differential data results in a large increase in rays near the focal region, thereby avoiding the partial distortion of the inversion model through focal dispersion and facilitating a finer velocity structure of the focal region compared to conventional seismic tomography (Yu et al., 2010; Wang et al., 2013b).

4. Data selection and model establishment

4.1. Data selection

The current study uses P waves from 4782 local (epicentral distance

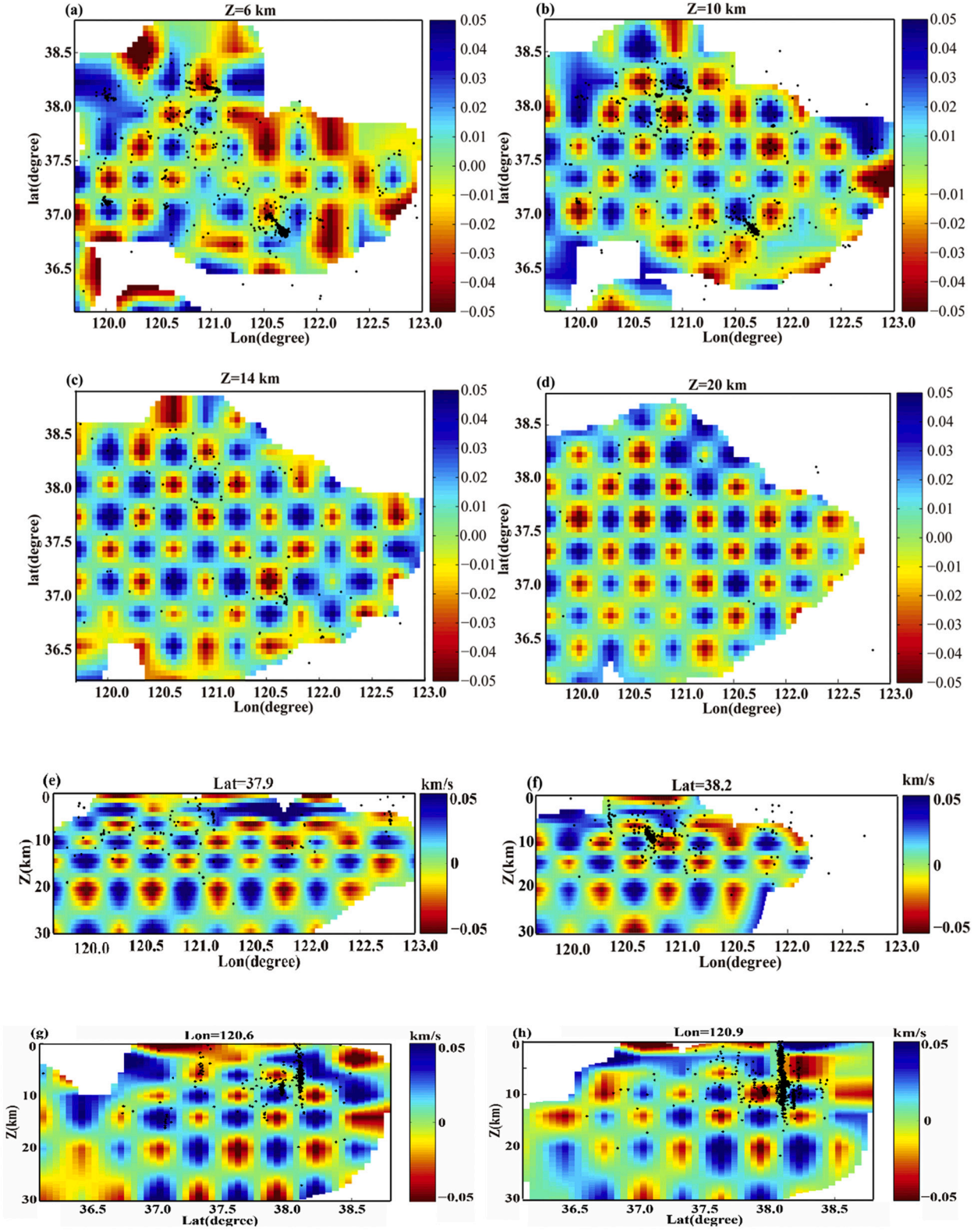

Fig. 5. Checkerboard test results for different depths and depth profiles along two latitudinal and two longitudinal lines.

≤400 km) events recorded by 34 stations in the JDP and 62 stations in the surrounding areas from January 2013 to January 2020. There are two important quality control steps in the data selection process. The first step is the quality of the seismic phase data used for the inversion. The selected events should have a clear first arrival-time and were recorded by at least four stations. The time-distance curves of P waves were used to eliminate phase data with errors exceeding 2 times the standard deviation. The second step is to optimize the linkage between the events and minimize redundancy in the travel-time difference data for pairs of earthquake at common stations. Ideally, a network of links is sought between events so that there exists a chain of pairwise connected events from any one event to any other event, with the distance being as

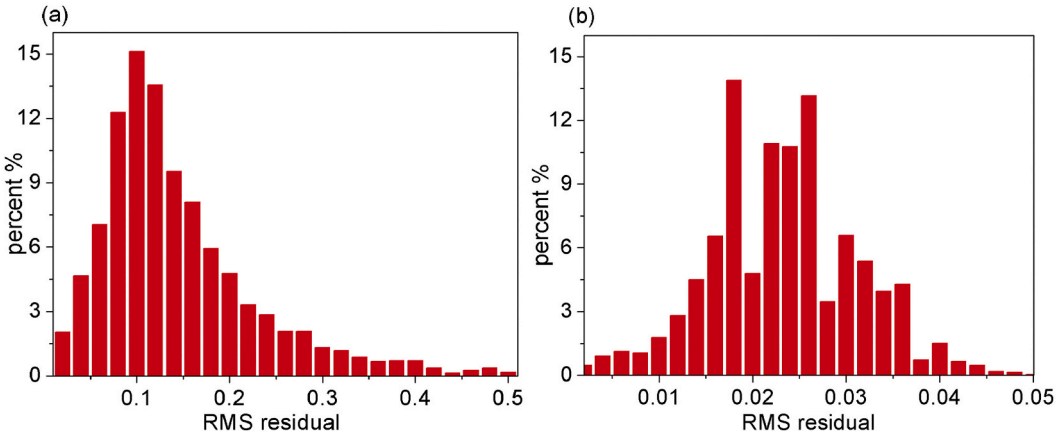

Fig. 6. Comparison of RMS travel time residuals before (a) and after (b) the relocation.

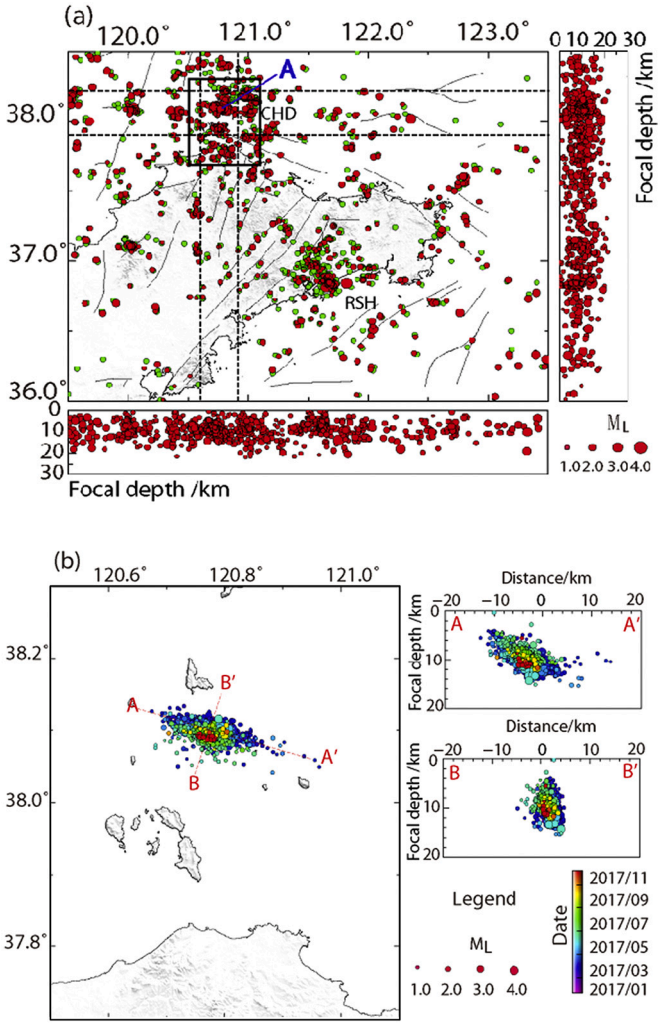

Fig. 7. Comparison of earthquake epicenters before and after relocation (a). CHD denotes the Changdao area, and RSH denotes the Rushan area. The two N-S and two *E*-W profiles in (a) indicate the locations of the cross-sections shown in Fig. 9. Depth profiles along the latitude and longitude directions are on both sides. (b), corresponding to the position A in the rectangle (a), shows the relocation results and profiles of 2017 Changdao earthquake swarm.

small as possible between connected events. The travel-time of two events to a same station with the same seismic phase is called a phase pair. The least number of seismic phase pairs of each event pair (two earthquakes) was set to eight, and the number of seismic phase pairs required for neighbors (two event pairs) was also set to eight. The current study only considered the "strongly link" seismic events in this area, a strong link is typically defined by eight or more observations (Waldhauser and Ellsworth, 2000). After the above screening, 2829 seismic events were finally selected and 81 stations participated in the inversion. The current study identified a total of 276,208 P wave seismic phase pairs, making up 51,567 correlating event pairs.

4.2. Model selection

A horizontally layered velocity model was used in the double-difference tomography. Because the initial velocity model has a significant influence on the three-dimensional inversion results, the ideal one-dimensional initial velocity model of the crust should be as close as possible to the actual crustal structure. Three initial velocity models were tested in this study (Fig. 2). Model 1 was based on the study of crustal velocity structure in the Shandong and adjacent areas (Wang et al., 2007; Su et al., 2016; Xu et al., 2016; Wang et al., 2017), and model 2 is the velocity model currently used in the Shandong Seismic Network for earthquake location. Both models were constructed by integrating the seismic velocities and the depths to the Conrad and Moho discontinuities from the previous tomographic studies. Model 3 was built based on results from an active source deep seismic sounding profile (Wang et al., 2013a; Pan et al., 2015; Li et al., 2015). Among the three models, Model 3 has the minimum RMS travel time residual (Model 1, 0.0264; Model 2, 0.0272; Model 3, 0.0245) and thus was selected as the initial model (Table 1) used in the inversion. To find the optimal block size and depth intervals, we conducted resolution tests (see the Resolution Test Section below for details) using three different grid sizes (0.2° × 0.2°, 0.3° × 0.3° , and 0.4° × 0.4°). The results show that a grid size of 0.3° × 0.3° gives the best resolution. The study area was therefore divided into 0.3° × 0.3° grids for the longitudinal range of 119.7° - 123.0°, and latitudinal range of 36.1° - 38.8°. The depths of 3, 6, 10, 14, 20, and 30 km were selected for the inversion.

4.3. Selection of regularization parameters

The variable quantity of slowness was constrained by smooth weighting during inversion, whereas the earthquake location and variable quantity of slowness were constrained by the damping factor. The sizes of the two parameters have a significant impact on the stability of the inversion result (Zhang and Thurber, 2006). The current study used the L-curve method (Hansen, 1992; Hansen and O'Leary, 1993) to

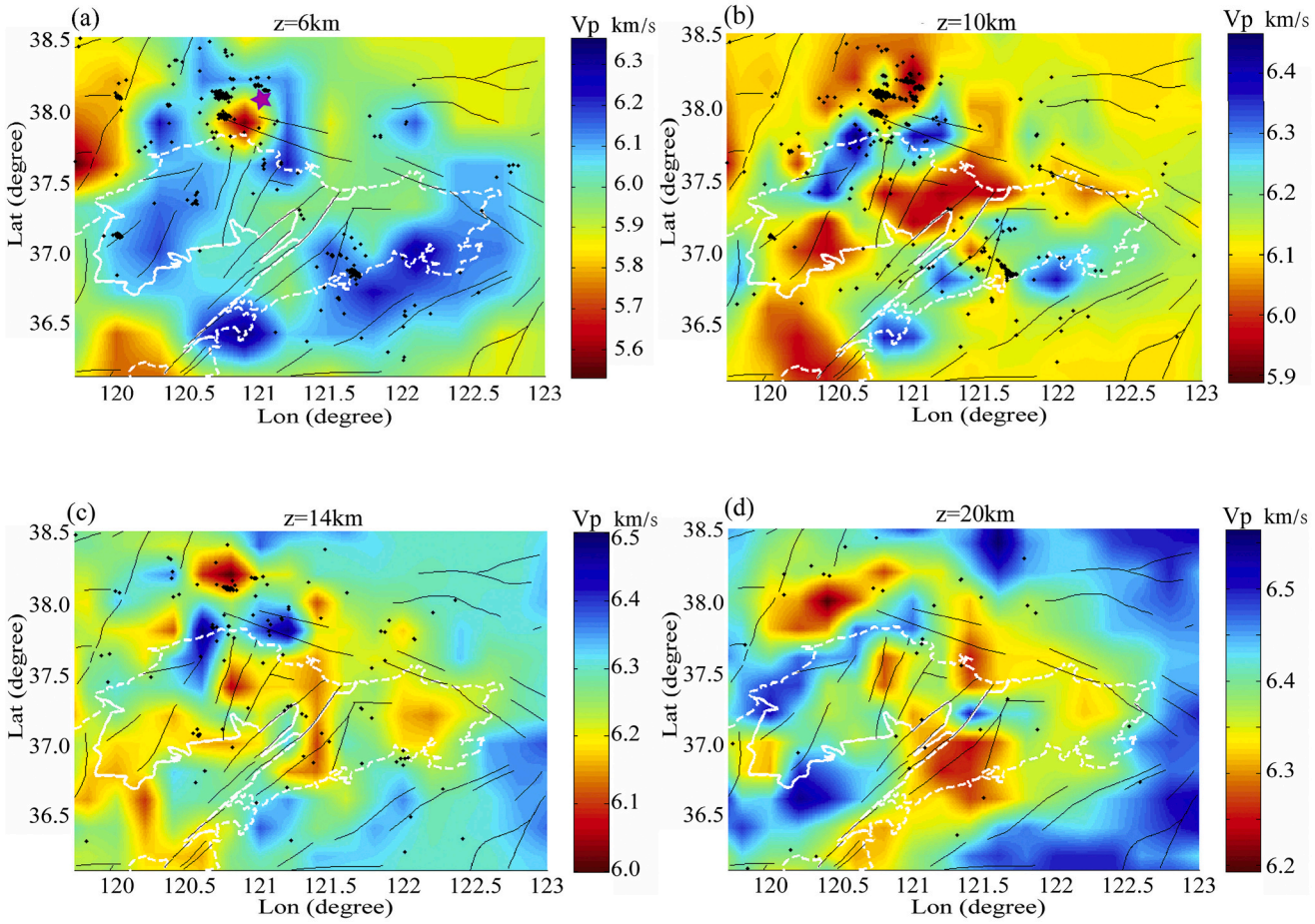

Fig. 8. P-wave velocity anomalies at different depths. Black solid lines denote faults, white chain-dotted lines denote unit structural boundaries, and black dots denote the projections of the relocated earthquakes plotted at the center of each layer. The purple star in (a) represents the 1548 Ms. 7.0 earthquake. (For interpretation of the references to colour in this figure legend, the reader is referred to the web version of this article.)

calculate the optimal parameter value. The search ranges of the smooth weight and damping factors were 1–200 and 30–700, respectively (Zhang and Thurber, 2006; Wang et al., 2015). Fig. 4a shows the normalized norm of the variable quantity of the slowness, whereas Fig. 4b shows that of earthquake location and the variability of slowness. An optimal smooth weight of 10 and damping factor of 200 were selected as the control parameters of the inversion process according to the relationship between the normalized model and the travel time residual.

5. Resolution test

Conditions such as the distributions of seismic events, stations, and seismic ray density affect the resolution of velocity structure inversion. The present study conducted a resolution test to evaluate the reliability and spatial resolution of the velocity image obtained from the inversion. Alternating positive and negative velocity perturbations of 5% were added to the inversion grid points of the initial one-dimensional velocity model to obtain the seismic detecting board of the initial 3D velocity. The synthetic travel time dataset was calculated according to the actual data. The velocity of the grid points was then inverted, and the resolution of each node was evaluated by comparing the resulting velocity of each node with the corresponding velocity in the input model. Since the earthquakes in this study are mainly concentrated in the depth range of 4 to 16 km, the test results showed that in the 6–20 km depth range, the area in which the rays were relatively concentrated, has a good inversion resolution (Fig. 5). In addition, the test results for the depth profiles along the latitude and longitude directions are also shown.

6. Results and discussion

6.1. Relocation results

The current study led to the relocation of 2780 earthquakes by isolating 2829 eligible events. The RMS (Root Mean Square) travel time residuals before the relocation are mainly distributed between 0.04 s and 0.2 s, with an average of ~0.1 s (Fig. 6a). After relocation, all the RMS travel time residuals are within 0.05 s whereas the mean is reduced to ~0.025 s, and therefore is an order of magnitude smaller than that before the relocation (Fig. 6b). Additionally, after the relocation, the epicenters became more concentrated in clusters with better defined dominant orientations, particularly for the Rushan and Changdao earthquake swarms. After the relocation of the Rushan earthquake swarm, the earthquakes form a NW-trending seismic zone of approximately 8 km long and 3 km wide, where no known seismic faults exist. Qu et al. (2019) provided a detailed description of the seismogenic structure of the Rushan earthquake sequence and speculated that the earthquake swarm may have occurred on a hidden fault. The results of the current study support this assertion.

Another recent earthquake swarm, the Changdao earthquake swarm, was located at the junction of the NWW and NE fault zones. After the relocation, the epicenters were more concentrated, forming a NWW-trending seismic zone of ~20 km long and ~ 10 km wide (Fig. 7b) that may largely be controlled by the Penglai-Weihai Fault and

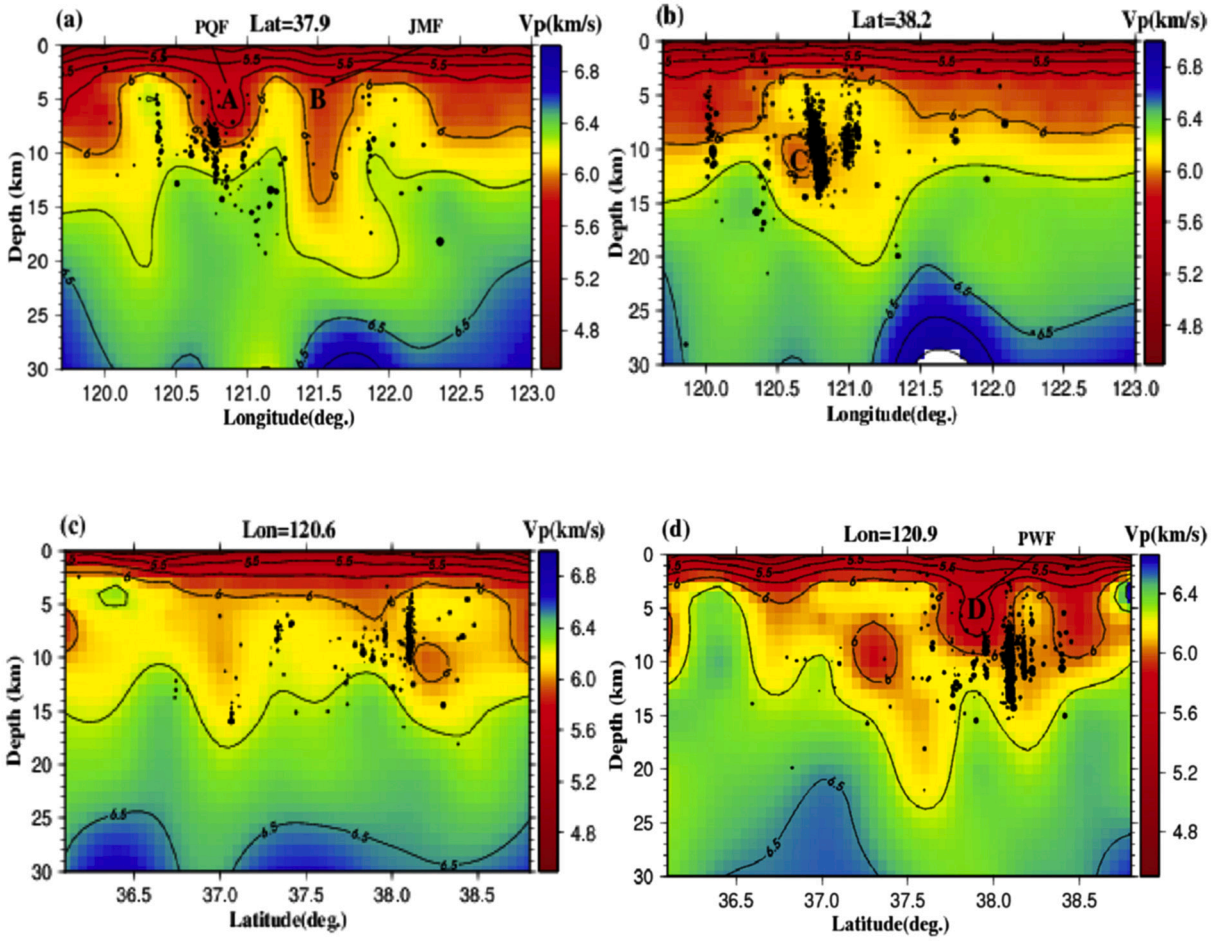

Fig. 9. Example N-S (top panel) and E-W (lower panel) vertical cross-sections of P-wave velocities. The location of the profiles can be found in Fig. 6a.

associated branch faults. This result is in accordance with those of a study by Li et al. (2019) on the earthquake swarm that occurred in February and September 2017. Li et al. (2019) speculated that the seismogenic fault may be located in the Dazhushan Island-Weihai Fault. Furthermore, the NE-trending Fengyidian, Qixia, Taocun, and Zhuwu faults and other faults in the study area were also found to be in good agreement with seismic activity, and the earthquakes showed linear distributions along most of the faults. In general, the relocated earthquakes demonstrated a significant correlation with the locations of faults, indicating that most of the fault zones in this area are currently active.

6.2. *Crustal P-wave velocity structure at different depths*

Fig. 8 shows the results of P-wave velocity imaging at the depths of 6 km, 10 km, 14 km and 20 km. In general, the majority of earthquakes in the study area occurred on the edges of or along the transition zones between high- and low-velocity bodies. For instance, at the depths of 6 km and 10 km, almost all the earthquakes in the Changdao area occurred around an isolated low-velocity body that has a nearly circular shape. In comparison, the Rushan earthquake swarm occurred in the transition zone between high- and low-velocity bodies. Previous studies (Michael and Eberhart-Phillips, 1991; Chiarabba and Amato, 2003; Kato et al., 2010) have shown that high-velocity bodies are generally comprised of high-strength rock masses, which are characterized by a higher level of brittleness and locally elevated ability to accumulate seismogenic energy, whereas low-velocity bodies are less rigid and are less capable of accommodating a large amount of strain energy. The transition zone between the high-velocity and low-velocity bodies can be an area of stress concentration, where the medium is relatively fragile and low in strength and thus is prone to earthquakes (Kato et al., 2010).

The velocity structures at different depths, which are in general agreement with the previous research results (Xu et al., 2009; Xu et al., 2016; Li et al., 2006b; Wang et al., 2017; Yu et al., 2020a, 2020b; Wei et al., 2020), indicate the existence of obvious lateral heterogeneity in the study area, especially between the Jiaobei Uplift, Jiaolai Basin and Sulu UHP Metamorphic Belt (Fig. 8). At shallow depth (6 km, Fig. 8a), lateral velocity variations correlate well with known near-surface geology (Fig. 1). Low-velocity anomalies appear in the sedimentary areas of the Jiaolai Basin, whereas high-velocity anomalies appear in mountainous regions (e.g., Jiaobei Uplift). This result is consistent with the S-wave velocity structure from ambient noise tomography (Li et al., 2018). The velocity beneath the Sulu UHP Metamorphic Belt is obvious higher than those of the Jiaobei Uplift and Jiaolai Basin (Fig. 8) at different depths, an observation that is consistent with the S-wave velocity result from ambient noise tomography (Li et al., 2018; Wei et al., 2020; Yu et al., 2020a) and seismic tomography results (Li et al., 2006a; Wang et al., 2017). In addition, since velocity is generally positively related to density, this conclusion is consistent with the fact that the Bouguer gravity anomaly in the Jiaobei Terrane (including Jiaobei Uplift and Jiaolai Basin) is obviously lower than that in Sulu UHP Metamorphic Belt (Yu et al., 2020a, 2020b).

The lateral variations of the resulting velocities correspond well spatially with the distribution of faults in the study area. The NNE-NE trending fault system is the most important fault structure in the JDP, and is most likely caused by the low-angle subduction of the paleo-Pacific Plate to the hinterland of the Asian continent during the Mesozoic (Tang et al., 2018). The plate convergence resulted in intensive

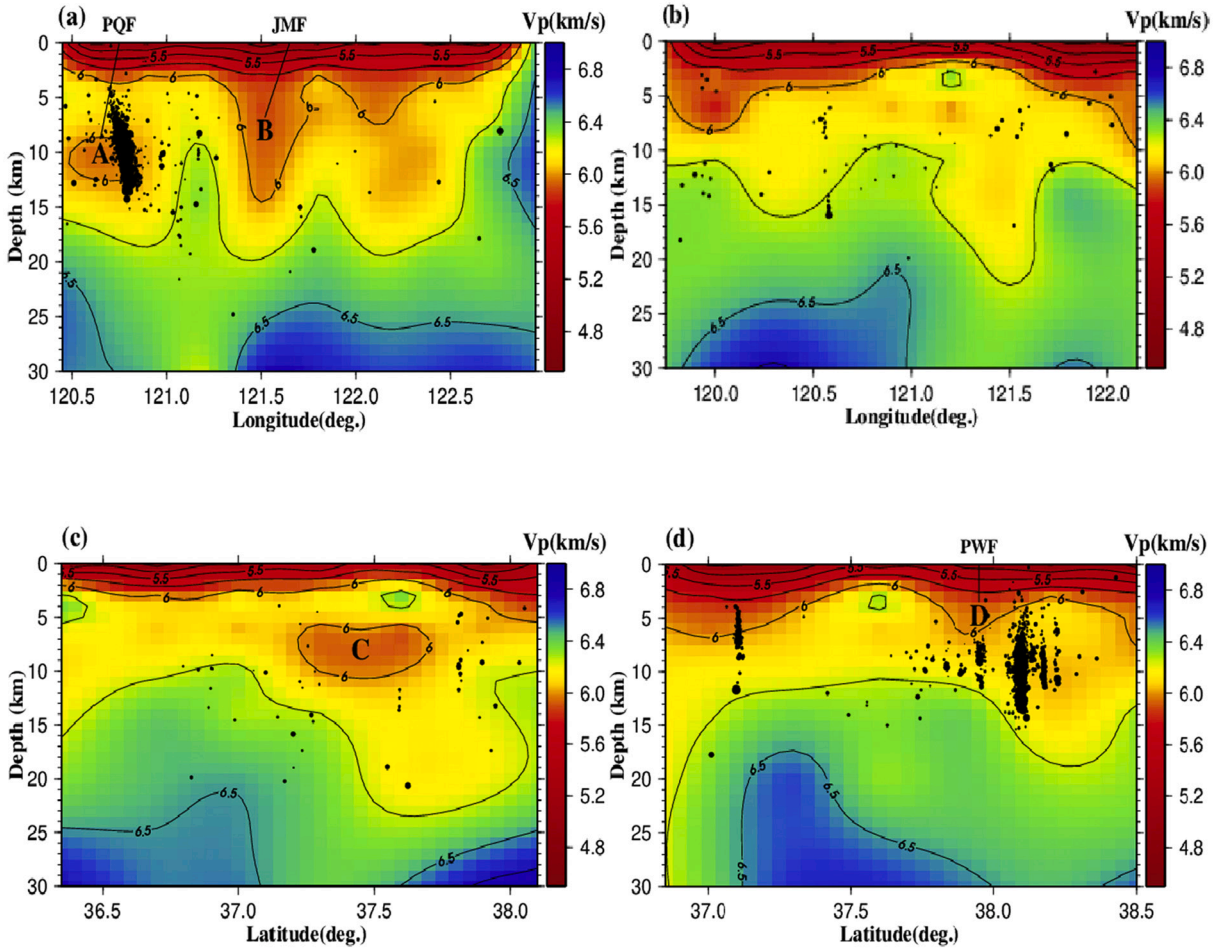

Fig. 10. Example NW (top panel) and NE (lower panel) oriented vertical cross-sections of P-wave velocities. The locations of the profiles are shown in Fig. 3.

compressive stress within the eastern part of North China, forming the NNE-NE-trending fold-fault tectonic system typical of eastern China, which controls the differential uplift of the blocks and the development of sedimentary basins (Isozaki, 1997; Maruyama et al., 1997; Zhai et al., 2004; Zhang et al., 2007; Zhang and Zhang, 2008). Vertical and horizontal displacements along the faults might have resulted in lateral variations in rock types and the physical properties of the same type of rocks, leading to the correspondence between the distributions of faults velocities. The Jiaobei Uplift is mainly composed of the Precambrian metamorphic rock series and Mesozoic granite, as well as small-scale Mesozoic and Cenozoic continental clastic-volcanic rocks, which are consistent with the high velocities observed at the shallow depths. The Jiaolai Basin mainly contains continental pyroclastic rocks intercalated with low-velocity sedimentary strata, and the Sulu UHP Metamorphic belt is well known for the occurrence of a large number of high-pressure/ultra-high pressure metamorphic rocks characterized by high velocity anomalies.

6.3. P-wave velocity structure in the vicinity of the Changdao earthquake swarm

To investigate the spatial relationship between velocity structure and earthquakes in the 2015–2018 Changdao earthquake swarm, in Fig. 9 we plot P-wave velocities along two N-S and two E-W vertical profiles traversing the swarm following a similar procedure used for investigating the Rushan earthquake swarm (Qu et al., 2015, 2019). Earthquakes within a 0.3° wide band centered at the profiles are also plotted to delineate the relationship between earthquake distribution and velocity structures, as shown in Fig. 8, the velocity structure diagrams of 6 km and 10 km suggest that most earthquakes in the swarm occurred around an obvious low-velocity body. This can be more clearly observed on the cross-sections as Anomaly A in Fig. 9a and Anomaly D in Fig. 9d. The depth of the anomaly gradually increases toward the north, extending to the middle-lower crust (C in Fig. 9b).

The low velocity body is located in the area where two groups of faults intersect. The NE-NNE trending Penglai-Qixia Fault Zone enters the North Yellow Sea to the north and intersects with the NWW-trending fault system (Fig. 1). There are four faults with a length ranging between 40 and 80 km from west to east, including the Beigou-Linglong, Fengyidian, Qixia and Bajiao-Shewobo faults (Fig. 1). The faults are parallel overall, with an interval of 10 km to 15 km and contain well-developed tectonic breccia, extruded lens and fault gouges (Huang et al., 2007). The spacing of the four faults (F1-F4 in Fig. 1) is comparable to the width of the observed low velocity anomaly (Figs. 7a and 8a). In addition, studies of acoustic detection (Wang et al., 2006) have shown that the Penglai-Weihai Fault Zone is composed of multiple NW-trending secondary faults, and that this zone remained active during the late Pleistocene. An Ms. 7.0 earthquake occurred at the intersection of the Beigou-Linglong Fault in the Penglai-Qixia Fault Zone and the Penglai-Weihai Fault in 1548 (Fig. 8). While some studies speculated that the NE-trending fault zone remains active in the sea area (Huang et al., 2007), other studies suggested that the earthquake occurred in the NW-trending fault zone (Deng et al., 2001; Wang et al., 2006).

Given the spatial correspondence between the location of the low velocity body (Anomaly A in Fig. 9a) and the area where the two groups of faults intersect, we speculate that Anomaly A is likely a fault fracture

zone formed by interweaving and cross-cutting of multiple NE- and NWW-trending faults. It has long been recognized that conjugate faults readily accumulate energy, and the development of a fault gouge can effectively reduce the friction of fault movement (Marone et al., 1990; Hirakawa and Ma, 2016), a mechanism that might be responsible for the more than 3000 recorded small earthquakes in the Changdao region since February 2017 (Fig. 7b). Earthquakes result in the readjustment of regional stress. The faults in the fracture zone do not readily accumulate energy, resulting in a concentration of energy mainly along the edge of the fracture zone. In contrast, since the marginal faults are more brittle and are oriented in different directions, they easily trigger new earthquakes during the continuous adjustment of stress. The results showed that there are earthquakes in both faults directions (Figs. 6 and 8), but the relocated earthquakes mainly followed a linear distribution of NWW-trending earthquake clustering, indicating that recent earthquakes should occur in the Penglai-Weihai Fault and in a series of NWW-trending secondary faults.

6.4. Vertical extent and geometry of fault zones

Because most major fault zones are characterized by low velocities and in some cases are boundaries of high or low velocity bodies, as discussed above, we next attempt to estimate the vertical extent and geometry of the faults by producing two NW and two NE oriented vertical cross-sections (Figs. 3 and 10) (earthquake projection follows the same procedure as Fig. 9). Fig. 10 suggests that the Mouping-Jimo Fault Zone (feature B in Fig. 10a) and Penglai-Qixia Fault Zone (feature A in Fig. 10a) extend northward and intersect with the Penglai-Weihai Fault Zone (feature C in Fig. 10c and feature D in Fig. 10d). From west to east, the Mouping-Jimo Fault Zone is mainly composed of four parallel and approximately equidistant faults, namely Taocun fault, Guocheng fault, Zhuwu fault, and Haiyang fault (Fig. 1). Due to the limitation of resolution, specific faults cannot be distinguished. However, by comparing the structural unit diagram (Fig. 1), the location of the faults in the horizontal velocity structure (Fig. 8b) and features in the profile (Figs. 9a and 10a), it is inferred that the Mouping-Jimo Fault Zone may be a major fracture cutting through the Earth's crust. It may also be the structural boundary zone between the Sulu UHP Metamorphic Belt and the Jiaobei Terrane (including Jiaobei Uplift and Jiaolai Basin) and a manifestation of the collision between the North China Block and the Yangtze Block. Some previous studies have reached the same or similar conclusions from observations of the depth and structure of the Moho, crustal Vp/Vs ratios, Bouguer gravity anomalies (Yu et al., 2020b), rock properties (Song and Wang, 2000; Zhang and Zhang, 2007), and velocity structure (Pan et al., 2015), while different conclusions have been reached by some other studies (Faure and Lin, 2001; Lin et al., 2003).

A fault zone manifests as a major fracture cutting through the Earth's crust. The ductile deformation in the lower part of the crust is more likely to transition to the brittle layer in the middle and upper parts of the crust (Scholz, 1988; Behr and Platt, 2014). The intersecting brittle transition zone becomes the epicenter of moderately-strong earthquakes under the action of regional stress (Pan et al., 2015). The Taocun Fault with an overall NNE 45° strike on the westernmost side of the Mouping-Jimo Fault Zone dips SE at an angle of 60°–80°. The Taocun Fault divides the Penglai-Weihai Fault Zone into east and west sections (Du, 2001; Wang et al., 2006). The east Yantai-Weihai section (C) was active during the Middle Pleistocene; there are relatively few secondary faults, but an Ms. 6.0 earthquake occurred in this section of the fault in 1948. The west Changdao-Yantai section (D) was active during the Late Pleistocene, and the structure of the fault zone is complex, with densely distributed numerous secondary faults and small earthquakes. Acoustic detection studies showed that both the Taocun and Haiyang faults extend to the northeast sea area, collectively forming a graben-like distribution, and the intersection of the NE-trending fault and the NW-trending fault is a favorable location for the occurrence of moderately-strong earthquakes (Wang et al., 2006).

7. Conclusions

The current study used 2829 seismic events recorded by the Shandong Seismic Network from 2013 to 2020 and the double-difference tomography method to invert the velocity structure of the JDP area. The following conclusions can be drawn based on the observations:

(1) After relocation, the residuals were reduced by an order of magnitude, and the epicenters became more concentrated in clusters with better defined dominant orientations, and the correspondence with known faults was more significant.
(2) Lateral velocity heterogeneities at different depths reflect variations in the physical properties of crustal rocks. Clear velocity contrasts have been identified between the Jiaobei Uplift, the Jiaolai Basin and the Sulu UHP metamorphic belt. Most of the velocity anomalies are NE-SW oriented, which is consistent with the general pattern of the fault structures observed in the JDP and reflects the control of fault structures on the regional geology.
(3) A large number of small and medium earthquakes have occurred in the Changdao area since February 2017, mainly due to the fracture zone formed by the intersection of the NE-trending Penglai-Qixia Fault Zone and the NWW-trending Penglai-Weihai Fault Zone. The edges of the fracture zone are prone to frequent earthquakes due to stress accumulation.
(4) It can be inferred that the Mouping-Jimo Fault Zone may be a crucial structural boundary zone between the Jiaobei Terrane and the Sulu Orogenic Belt. The Mouping-Jimo fault zone extends northward and intersects with the Penglai-Weihai Fault Zone. The area where the two fault systems intersect has the potential of producing moderate-strong earthquakes.

Declaration of Competing Interest

None.

Acknowledgments

We used data from the Shandong Earthquake Network, and we are grateful to all colleagues and team members for their efforts of obtaining the phase data. We would like to thank Dr. Haijiang Zhang for providing the tomoDD Program, and Dr. Tuo Wang, Mr. Kailun Ba, Mr. Yanwei Zhang, Mr. Enbo Fan at Missouri University of Science and Technology for their assistance in reformatting the data set and inspiring discussions. We also thank the editor, Dr. Lin Chen, and three anonymous reviewers for their constructive comments and suggestions, which significantly improved the quality of this paper. This work was supported by an Earthquake Science and Technology Stimulation Project (XH19027) funded by the China Earthquake Administration, China Scholarship Council (201904190008) and Natural Science Foundation of Shandong Province (ZR2020KF003).

References

Behr, W.M., Platt, J.P., 2014. Brittle faults are weak, yet the ductile middle crust is strong: Implications for lithospheric mechanics. Geophys. Res. Lett. 41 https://doi.org/10.1002/2014GL061349.
Chiarabba, C., Amato, A., 2003. Vp and Vp/Vs images in the Mw6.0 Colfiorito fault region (central Italy): a contribution to the understanding of seismotectonic and seismogenic processes. J. Geophys. Res. 108 https://doi.org/10.1029/2001JB001665.
Deng, Q.D., Min, W., Chao, H.T., 2001. Cenozoic tectonic and seismologic activities in Bohai Sea. In: Neotectonics and Environment. Seismologic Press, Beijing.
Du, G.Y., 2001. Subsection of the active structure of Weihai-Penglai. J. Geol. Hazards Environ. Preserv. 12, 15–18.
Du, G.Y., Wang, Q., Sun, Q.Y., 2001. Statistical analysis of the river networks on neotectonic divergency of east and west parts in Jiaodong Peninsula. Acta Sci. Nat. Univ. Pekin. 37, 407–412.
Fan, H.R., Hu, F.F., Yang, J.H., Shen, K., Zhai, M.G., 2005. Fluid evolution and large-scale gold metallogeny during Mesozoic tectonic transition in the eastern Shandong province. Acta Petrol. Sin. 21, 1317–1328.

Faure, M., Lin, W., 2001. Where is the North-South China block boundary in eastern China? Geology. 29, 119–122.
Ge, J., Zhang, Z.K., Ni, J.L., Han, S., Hou, X.H., Li, M., 2015. Features and dynamic mechanism of the southern end of Muping-Jimo Fault. Geoscience 29, 747–754.
Guo, J.H., Chen, F.K., Zhang, X.M., SiEbel, W., Zhai, M.G., 2005. Evolution of syn-to post-collisional magmatism from North Sulu UHP belt, eastern China: zircon U-Pb geochronology. Acta Petrol. Sin. 21, 1281–1301.
Hansen, P.C., 1992. Analysis of discrete ill-posed problem by means of the L-curve. SIAM Res. 34 (4), 561–580.
Hansen, P.C., O'Leary, D.P., 1993. The use of the L-curve in the regularization of discrete ill-posed problems. SIAM J. Sci. Comput. 14, 1487–1503.
Hirakawa, E., Ma, S., 2016. Dynamic fault weakening and strengthening by gouge compaction and dilatancy in a fluid-saturated fault zone. J. Geophys. Res. Solid Earth 121, 5988–6008. https://doi.org/10.1002/2015JB012509.
Huang, Y.H., You, H.C., Song, Y.S., Guo, Y.G., Huan, W.L., 2007. Recent activities of faults in Jiaodong Peninsula, Shandong Province, China. Technol. Earthq. Disast. Prev. 2, 39–49.
Isozaki, Y., 1997. Jurassic accretion tectonics of Japan. Island Arc 6, 25–51.
Kato, A., Moyatake, T., Hirata, N., 2010. Asperity revealed barriers of the 2004 Mid-Niigata prefecture earthquake revealed by highly dense seismic observations. Bull. Seismol. Soc. Am. 100, 298–306.
Li, B., Cui, X., Zhang, Z.H., Cai, Y., Ji, A.D., 2019. Research on the repositioning and seismic source characters of the changdao coastal earthquake sequences, Shandong Province. Technol. Earthq. Disast. Prev. 14, 108–117.
Li, C.L., Chen, C.X., Dong, D.D., Kuponiyi, A.P., Dosso, S.E., Su, D.L., 2018. Ambient noise tomography of the Shandong province and its implications for Cenozoic intraplate volcanism in Eastern China. Am. Geophys. Union. https://doi.org/10.1029/2018GC007515.
Li, J.J., Luo, Z.K., Yan, C.H., Xie, R.B., Li, D.S., Li, H.K., Luo, H., Liu, X.Y., Liu, X.X., Li, S., 2010. Structure framework and evolution of the North China craton. Contrib. Geol. Min. Resourc. Res. 25, 89–100.
Li, J.W., Vasconcelos, P., Zhou, M.F., Chang-Qian Ma, C.Q., 2006a. Geochronology of the Pengjiakuang and Rushan gold deposits, eastern Jiaodong gold province, northeastern China: implications for regional mineralization and geodynamic setting. Econ. Geol. 101, 1023–1038.
Li, Z.H., Zheng, Y.P., Zhi, P.Y., Liu, B.H., Hao, T.Y., Zhang, X.H., Liu, C.G., Ma, L., 2015. The new progress of deep seismic survey and crustal structure in southeast of Bohai Sea-based on the data processing and analysis of OBS2013line. Prog. Geophys. 30, 1402–1409.
Li, Z.W., Xu, Y., Hao, T.Y., Liu, J.S., Zhang, L., 2006b. Seismic tomography and velocity structure in the crust and upper mantle around Bohai Sea area. Chin. J. Geophys. 49, 794–804.
Lin, W., Michel, F., Wang, Q.C., 2003. Mesozoic geometry and kinematics in the Jiaodong peninsula and its tectonic evolution. Chin. J. Geol. 38, 495–505.
Ma, X.Y., 1989. Lithospheric Dynamics Atlas of China. China Cartographic Publication House, Beijing.
Marone, C., Raleigh, C.B., Scholz, C.H., 1990. Frictional behavior and constitutive modeling of simulated fault gouge. J. Geophys. Res. 95 (B5), 7007–7025.
Maruyama, S., Isozaki, Y., Kimura, G., Masaru, T., 1997. Paleogeographic maps of the Japanese Islands: plate tectonic synthesis from 750 Ma to the present. Island Arc 6, 121–142.
Meng, Q.R., 2003. What drove late Mesozoic extension of the northern China–Mongolia tract? Tectonophysics 369, 155–174.
Michael, A.J., Eberhart-Phillips, D., 1991. Relations among fault behavior, subsurface geology, and three-dimensional velocity models. Science 253, 651–654.
Paige, C.C., Saunders, M.A., 1982. LSQR: Spare linear equations and least squares problems. ACM Trans. Math. Softw. 8, 195–209.
Pan, S.Z., Wang, F.Y., Zheng, Y.P., Duan, Y.L., Liu, L., Deng, X.G., Song, X.H., Sun, Y.N., Ma, C.J., Li, Y.Q., 2015. Crustal velocity structure beneath Jiaodong Peninsula and its tectonic implications. Chin. J. Geophys. 58, 3251–3263.
Qiu, L.G., Ren, F.L., Cao, Z.X., Zhang, Y.Q., 2008. Late Mesozoic magmatic activities and their constraints on geotectonics of jiaodong region. Geotecton. Metallog. 32, 117–123.
Qu, J.H., Jiang, H.K., Li, J., Zhang, Z.H., Zheng, J.C., Zhang, Q., 2015. Preliminary study for seismogenic structure of the Rushan earthquake sequence in 2013-2014. Chin. J. Geophys. 58, 1954–1962.
Qu, J.H., Wang, C.Z., Liu, F.B., Zhou, S.H., Zheng, J.C., Li, X.F., Zhang, Q., 2019. Study on relationship between seismic distribution of Rushan sequence and velocity structure. Seismol. Geol. 41, 99–118.
Scholz, C.H., 1988. The brittle-plastic transition and the depth of seismic faulting. Geol. Rundsch. 77, 319–328.
Song, M.C., 2008. Tectonic Framework and tectonic Evolution of the Shandong Province. Chin. Acad. Geol. Sci. Doctor. Degree 193.
Song, M.C., Wang, L.M., 2000. The latest understandings of fundamental geology of Jiaonan orogenic belt. Region. Geol. China 19, 1–6.
Song, M.C., Wan, G.P., Cao, C.G., He, C.Y., 2012. Geophysical-geological interpretation and deep-seated gold deposit prospecting in Sanshandong-Jiaojia area, eastern Shandong Province, China. Acta Geol. Sin. 86, 640–652.
Su, D.L., Fan, J.K., Wu, S.G., Chen, C.X., Dong, X.N., Chen, S.J., 2016. 3D P-wave velocity structures of crust and their relationship with earthquakes in the Shandong area. Chin. J. Geophys. 59, 1335–1349.
Tang, H.F., Cheng, R.H., Bai, Y.F., Kong, Q.Y., 2003. Tectonic evolution of the Jiaolai Basin. Glob. Geol. 22, 246–251.
Tang, J., Zheng, Y.F., Wu, Y.B., Gong, B., Liu, X.M., 2007. Geochronology and geochemistry of metamorphic rocks in the Jiaobei terrane: constraints on its tectonic affinity in the Sulu orogen. Precambrian Res. 152, 48–82.
Tang, J., Xu, W., Wang, F., Ge, W., 2018. Subduction history of the Paleo-Pacific slab beneath Eurasian continent: mesozoic-paleogene magmatic records in Northeast Asia. Sci. China-Earth Sci. 61, 527–559.
Um, J., Thurber, C., 1987. A fast algorithm for two-point seismic ray tracing. Bull. Seismol. Soc. Am. 77, 972–986.
VanDecar, J.C., Crosson, R.S., 1990. Determination of teleseismic relative phase arrival times using multi-channel cross-correlation and least squares. Bull. Seismol. Soc. Am. 80, 1548–1560.
Waldhauser, F., Ellsworth, W.L., 2000. A double-difference earthquake location algorithm: Method and Application to the Northern Hayward fault. Bull. Seismol. Soc. Am. 90, 1353–1368.
Wang, C.Z., Wu, J.P., Fang, L.H., Wang, W.L., 2013b. The relationship between wave velocity structure around Yushu earthquake source region and the distribution of aftershocks. Chin. J. Geophys. 56, 4072–4083.
Wang, F.Y., Zhang, X.K., Chen, Y., Li, L., Chen, Q.F., Zhao, J.R., Zhang, J.S., Liu, B.F., 2004. 2-D P-wave velocity structure in the mideast segment of Zhangjiakou-Bohai tectonic zone: Anxin-Xianghe-Kuancheng DSS Profile. Acta Seismol. Sin. 17, 31–41.
Wang, G.J., Teng, J.W., Zhang, X.K., 2007. The crustal structure of western Shandong and the high-velocity body in the crust. Chin. J. Geophys. 50, 1480–1487.
Wang, S., Xu, Y., Meng, X.C., 2017. Tomographic images of crustal structure beneath the Bohai Strait and surrounding areas, eastern China. Chin. J. Geophys. 60, 112–122.
Wang, S.J., Wang, F.Y., Zhang, J.S., Zheng, Y.P., Zhang, C.K., Zhao, J.R., Liu, B.F., Huang, C., 2013a. Crustal structure and its features in the southwest margin of Bohai Bay and adjacent areas. Seismol. Geol. 35, 278–289.
Wang, X.N., Yu, X.W., Zhang, W.B., 2015. 3D P-wave velocity structure of the crust and relocation of earthquakes in the Lushan source area. Chin. J. Geophys. 58, 1179–1193.
Wang, Z.C., Deng, Q.D., Chao, H.T., Du, X.S., Shi, R.H., Sun, Z.M., Xiao, L.X., Min, W., Ling, H., 2006. Shallow depth sonic reflection profiling studies on the active Penglai-Weihai fault zone offshore of the northern Shandong peninsula. Chin. J. Geophys. 49, 1092–1101.
Wei, Z.G., Chu, R.S., Chen, L., Wu, S.S., 2020. Crustal structure in the middle-southern segments of the Tanlu Fault Zone and adjacent regions constrained by multifrequency receiver function and surface wave data. Phys. Earth Planet. Interiors 201 (2020), 1–13, 106470.
Xia, Z.M., Liu, J.l., Ni, J.l., Zhang, T.T., Shi, X.M., Wu, Y., 2016. Structure, evolution and regional tectonic implications of the Queshan metamorphic core complex in eastern Jiaodong Peninsula of China. Sci. China Earth Sci. 59, 997–1013.
Xu, Y., Li, Z.W., Kim, K., Hao, T.Y., Liu, J.S., 2009. Crustal velocity structure and collision boundary between the Sino-Korea and Yangtze blocks in the Yellow Sea. Chin. J. Geophys. 52, 646–652.
Xu, Y., Wang, S., Meng, X.C., 2016. Tomographic evidence of the Tan-Lu fault zone in the Bohai Sea of eastern China. Sci. China Press 61, 891–900.
Yu, G.P., Xu, T., Liu, J.T., Ai, Y.S., 2020a. Late Mesozoic extensional structures and gold mineralization in Jiaodong Peninsula eastern North China Craton: an inspiration from ambient noise tomography on data from a dense seismic array. Chinese J. Geophys. 63, 1878–1893.
Yu, G.P., Xu, T., Ai, Y.S., Chen, L., Yang, J.H., 2020b. Significance of crustal extension and magmatism to gold deposits beneath Jiaodong Peninsula, eastern North China Craton: seismic evidence from receiver function imaging with a dense array. Tectonophysics 789 (2020), 1–13, 228532.
Yu, X.W., Chen, Y.T., Zhang, H., 2010. Three dimensional crustal P—wave velocity structure and seismicity analysis in Beijing Tianjin Tangshan Region. Chin. J. Geophys. 53, 1817–1828.
Zhai, M.G., Meng, Q.R., Liu, J.M., Hou, Q.L., Hu, S.B., Li, Z., Zhang, H.F., Liu, W., Shao, J. A., Zhu, R.X., 2004. Geological features of Mesozoic tectonic regime inversion in Eastern North China and implication for geodynamics. Earth Sci. Front. 11, 285–297.
Zhang, H.J., Thurber, C.H., 2003. Double-difference tomography: the method and its application to the Hayward fault, California. Bull. Seismol. Soc. Am. 93, 1875–1889.
Zhang, H.J., Thurber, C.H., 2006. Development and applications of double-difference seismic tomography. Pure Appl. Geophys. 163, 273–403.
Zhang, K., Lü, Q.T., Yan, J.Y., Hu, H., Fu, G.M., Shao, L.S., 2018. Crustal structure beneath the Jiaodong Peninsula, North China, revealed with a 3D inversion model of magnetotelluric data. J. Geophys. Eng. 15, 2442–2454.
Zhang, T., Zhang, Y.Q., 2007. Geochronological sequence of mesozoic intrusive magmatism in Jiaodong Peninsula and its tectonic constraints. Geol. J. China Univ. 13, 323–336.
Zhang, T., Zhang, Y.Q., 2008. Late Mesozoic tectono-magmatic evolution history of the Jiaobei uplift, Jiaodong peninsula, Shandong Peninsula. Acta Geol. Sin. 82, 1210–1228.
Zhang, Y.Q., Dong, S.W., Shi, W., 2003. Cretaceous deformation history of the middle Tan-Lu fault zone in Shandong Province, eastern China. Tectonophysics 363, 243–258.
Zhang, Y.Q., Li, J.L., Zhang, T., Yuan, J.Y., 2007. Late mesozoic kinematic history of the muping-jimo fault zone in Jiaodong Peninsula, Shandong Province, East China. Geol. Rev. 53, 289–300.
Zhao, Z., Zhao, Z.X., Xu, J.R., 2012. Velocity structure heterogeneity and tectonic motion in and around the Tan-Lu fault of China. J. Asian Earth Sci. 57, 6–14.